INL/CON-07-13535
PREPRINT

General and Localized Corrosion of Borated Stainless Steels

NACE Corrosion 2008

T. E. Lister
R. E. Mizia
A. W. Erickson
B. S. Matteson

March 2008

The INL is a
U.S. Department of Energy
National Laboratory
operated by
Battelle Energy Alliance

GENERAL AND LOCALIZED CORROSION OF BORATED STAINLESS STEELS

T.E. Lister, R.E. Mizia, A.W. Erickson, and B.S. Matteson
Idaho National Laboratory
P.O. Box 1625
Idaho Falls, Idaho 83415

ABSTRACT

The Transportation, Aging and Disposal (TAD) canister-based system is being proposed to transport and store spent nuclear fuel at the Monitored Geologic Repository (MGR) located at Yucca Mountain, Nevada. The preliminary design of this system identifies borated stainless steel as the neutron absorber material that will be used to fabricate fuel basket inserts for nuclear criticality control. This paper discusses corrosion test results for verifying the performance of this material manufactured to the requirements of ASTM A887, Grade A, under the expected repository conditions.

Keywords: borated stainless steel, localized corrosion, secondary phase, Yucca Mountain, neutron poison

INTRODUCTION

The Yucca Mountain Project (YMP) was directed by the Department of Energy Office of Civilian Radioactive Waste Management (DOE-RW) to develop a new repository waste package design based on the transport, aging, and disposal (TAD) canister system concept.[1] The waste package is the disposal container that the TAD canister will be sealed inside prior to its disposal in the repository. A neutron poison material for fabrication of the internal spent nuclear fuel (SNF) baskets for these canisters is required. The specified criticality control material for this system is borated stainless steel manufactured to the requirements of ASTM A887-89, Grade A, Type 304B4.[2] Eight alloy types based on a base 304 stainless steel with a B addition are specified in ASTM A887 from 304B (0.20-0.29% B) to 304B7 (1.75-2.25% B). Borated stainless steel has been used for criticality control for the wet storage and transportation of SNF.[3,4] The ASTM A 887 specification does not explicitly state the manufacturing methods but is based on mechanical property minimums. To meet the requirements of the Grade A specification, the alloys have been manufactured by a powder metallurgy process and the Grade B materials are based on ingot metallurgy. One heat of material tested (A978) was produced by ingot metallurgy techniques.

Borated stainless steel alloys solidify as primary austenite with a terminal eutectic constituent, which has the form Fe_2B, Cr_2B, with the exact composition dependent on the initial boron level.[5] The austenite matrix is a ductile phase, and the dispersed secondary phase is a comparatively brittle compound. In general, the powder-metallurgy product (Grade A) will have smaller, more circular borides than the ingot-metallurgy product, which will improve mechanical properties (impact strength and tensile ductility).[6]

The corrosion behavior of borated stainless steels is significantly different than austenitic stainless steels due to the presence of the secondary phase. Attack of the regions surrounding the particles has been attributed to a depletion of chromium at these regions.[7] This depletion was confirmed by electrolytic intergranular corrosion tests.[7] The same paper reported deep pitting corrosion for electrochemical polarization tests in NaCl solutions. The pits were reported to nucleate at secondary phase particles. Grade B materials are known to have lower corrosion resistance due to the larger irregular particle distribution.[8] Long-term immersion testing of Grade B materials has been performed to evaluate the corrosion performance versus witness austenitic materials in simulated concentrated ground water solutions at 90ºC.[9] Overall, these tests showed extensive localized corrosion for the Grade B materials in comparison to the witness austenitic materials.

Corrosion testing of both powder and ingot metallurgy products has been conducted to determine the stability of the materials in environments expected inside a breeched waste package during the 10,000 years after MGR closure. A discussion of this work is presented below. Note that a comparison of performance between borated stainless steels and another type of neutron absorbing alloy, Ni-Cr-Mo-Gd alloy will be presented at this meeting in Paper 08592.

EXPERIMENTAL

Specimens

Table 1 shows the composition of the alloys used for testing. Ingot metallurgy (A978) specimens were refinished from coupons previously used for the YMP corrosion studies (culled for the least amount of damage) by Lawrence Livermore National Laboratory (LLNL) (Heat E084295).[9] This was the specified material for the YMP waste package SNF baskets at the start of these tests. These specimens had been used for long-term immersion tests and were not designed for electrochemical testing. The size of the furnished specimens did not allow fabrication of the crevice specimens used for the other alloys. These specimens were used due to the lack of availability of untested material.

Specimens of Types 304B4, 304B5, and 304B6 Grade A alloys were machined from plate stock. To ensure that only the borated stainless steel matrix was tested, the as-received plate (304B4, 304B5, 304B6,) had the hot isostatic press can material (Type 304 stainless steel) removed from the top and bottom surfaces. The electrochemical crevice specimens for the Grade A specimens were 0.75 in. (1.9 cm) × 0.75 in (1.9 cm) × 0.375 in (0.95 cm), with a 0.28-in. (0.71 cm) through-hole for the crevice assembly. The A978 specimens obtained from LLNL were approximately 1 in. (2.5 cm) × 1 in. (2.5 cm) × 0.125 in. (0.32 cm), with a 0.3-in. (0.76 cm) through-hole for the crevice assembly. The specimens were wet sanded with 240- and 600-grit SiC paper the day of testing.

The crevice formers used in the test were ceramic multiple crevice assembly (MCA)-type. The surfaces were wet sanded with 600-grit SiC paper to smooth the as-received surfaces. The crevice formers were attached to the specimens with fasteners made of Ni-Cr-Mo alloy N10276. Polytetrafluoroethylene (PTFE) tape was wrapped on the crevice bolt to electrically isolate it from the specimen. A torque of 50 in-oz was applied to the crevice bolt for all tests. PTFE MCA washers were used with the as-received finish in select experiments to determine the effect of the crevice former material.

A special electrical contact was needed for the A978 specimens (originally machined to be exposure coupons) due to the lack of width for a conventional attachment. A short platinum wire was spot-welded to the specimen surface, and an electrical lead wire was soldered to the platinum wire. This contact was coated with water resistant epoxy to prevent solution contact.

Solutions

The compositions of the two solutions used in these tests are shown in Table 2. These solutions are based on expected compositions (major ions) for in-package chemistry. Each solution was mixed in a large batch using sodium salts, such that all solutions of that type were the same. Chemicals were American Chemical Society (ACS) grade used exclusively for this work. The nitrate-to-chloride and nitrate-to-halide ratios are calculated for comparison purposes. A higher value would be considered a less aggressive solution.

Electrochemical cell

The cell was similar to that described in ASTM G5, Figure 3.[10] All tests were performed at 60°C, maintained by a thermocouple-based temperature controller. The heating was supplied by a mantle under the cell. The temperature of the cell was confirmed using a calibrated thermometer before the initiation of each test. The cell was fitted with a condenser to prevent solution loss during the test. Chilled water (5°C) was passed through the condenser jacket. The reference electrode was contained in a water-jacketed Luggin capillary to keep the reference near room temperature. All testing utilized a saturated calomel electrode (SCE). All values are presented versus an SCE electrode. A single graphite rod was employed as the counter electrode.

Cyclic potentiodynamic polarization tests

Cyclic potentiodynamic polarization (CPP) tests were performed in solution B1 as a preliminary investigation of the corrosion properties of these materials. These tests were performed to be consistent with ASTM G5 testing protocols. A cyclic potential profile was used to investigate the repassivation characteristics of the materials on the return sweep. Heat E084295 was used for the A978 specimen. The CPP test was initiated after performing a 50-min corrosion potential (E_{corr}) measurement with N_2 purge. The solution was purged with N_2 during the entire test period. The CPP scan was initiated -0.2 V negative of the measured E_{corr} and reversed at +0.8 V versus a SCE. The scan rate was 0.166 mV/sec.

Potentiostatic tests

Potentiostatic (PS) tests were used to determine the corrosion performance of the alloys over longer periods. PS tests reported here were performed on specimens of 304B4, 304B5, and 304B6 using the following protocol: (1) measurement of E_{corr} under aeration for 24 hours, (2) measurement of E_{corr} under N_2 purge for 24 hours, (3) followed by three LPR scans, and (4) 7-day PS hold at 0.1 V versus SCE. The testing was performed in solution B3.

Three LPR measurements were made just prior to the PS tests. These tests were performed after N_2 degassing for 24 hours. The scans were performed at 0.166 mV/sec from -30 mV to +30 mV versus the measured E_{corr}. The corrosion current (i_{corr}) was calculated using ASTM G59 Equation 2. The Stern-Geary constant (B) was estimated using Tafel slopes of 0.120 V/dec (B = 0.0261 V). The corrosion rate was calculated from i_{corr} as described above ASTM G102.[11]

PS tests were performed under N_2 purge for a period of 7 days. A corrosion rate was determined using the current value for the last data point. This corrosion rate assumes a uniform removal of materials. As localized corrosion by definition is not a uniform mechanism, the rate will not have the same meaning, but it is still proportional to the amount of material being removed. The corrosion rate was calculated from the measured i_{corr} using ASTM G102.[11]

Long-term E_{corr} tests

To determine the long-term E_{corr} value under aeration for 304B4 and 304B5 specimens, the E_{corr} was measured continuously for four consecutive 1-week periods at 60°C. Short gaps exist (up to several hours) where data was not collected. Deionized water was added to replace the water loss on a weekly basis thus diluting the ion concentration slightly over the testing period.

Post-test analysis

Photography, light optical microscopy (LOM), and scanning electron microscopy (SEM) were used to capture the surface morphology of the surface after testing. The SEM was used in backscatter (BSE) and secondary (SE) modes. BSE mode allows the secondary phase (dark grey) to be differentiated from the austenite phase (lighter color). Optical profile microscopy (OPM) was used to obtain three-dimensional profiles of the specimen surface after testing. Examination of corrosion products collected from specimens or the bottom of the flask was performed using conventional x-ray diffraction (XRD).

RESULTS

Cyclic potentiodynamic polarization tests

CPP measurements were performed for all four alloys using ceramic MCA washers in B1 solution. Figure 1 shows CPP scans for the A978 and 304B4 specimens. The vertical dotted line in Figure 1 indicates the breakdown threshold using a 10 $\mu A/cm^2$ criterion. Table 3 contains parameters obtained from the corrosion potential (E_{corr}) and CPP curves for all four alloys. Note that the 304B5 has the most positive breakdown potential (E_{bd}), and the repassivation potential (E_{rp}) value is very similar to 304B4 (best performing). This observation is consistent with the low number of negative spikes in the aerated E_{corr} measurements for 304B5 as will be shown in Figure 4 and 8 below. The

A978 specimen had the most negative values for E_{bd} and E_{rp} (worst performing). The 304B6 had a similar E_{bd} to 304B4 but has a much more negative E_{rp} that is similar to the A978. Because the 304B6 has significantly more B content than A978, the similar E_{rp} value indicates a microstructural effect. Thus, these tests show that the amount of boron and the alloy grade (microstructure) significantly influences the localized corrosion characteristics of these alloys. In all cases, significant pitting was observed under the crevice formers. In some cases, pitting was observed on boldly exposed surfaces as well.

Additional CPP tests were performed for the three Grade A alloys in solution B3 using PTFE MCA crevice formers. The curves from these tests are shown in Figure 2, with the data tabulated in Table 4. The E_{corr} values follow the trend of decreasing with increasing boron level. The E_{bd} potentials do not follow the trend of boron content because 304B5 has a higher E_{bd} value than 304B4. The E_{rp} values decrease with increasing boron level, as expected. A comparison of the alloys in the two solution types shows only a slight depression of the E_{corr} and E_{rp} values in B3, which is a significantly lower NO_3/(Cl+F) value. The E_{bd} values are actually higher in the B1 solution, which is counter to the expected effect of halides. It is thought that at these low ionic contents the concentration of halides, which contribute to enhanced corrosion, must be less of an influence in localized corrosion processes. More testing would be required to make any significant statements about these results because they are based on single observations.

Figure 3 shows a photograph of a 304B4 specimen following CPP testing. The light colored areas are regions under the ceramic MCA where crevice corrosion had occurred. As can be seen, approximately a third to a half of the crevice formers showed significant crevice corrosion. This was type of damage was typical of all the specimens with the A978 specimen having almost all the crevice formers showing significant corrosion.

Potentiostatic tests

PS testing was performed on Grade A specimens with ceramic MCA washers to determine the effect of B on the corrosion characteristics at values near the expected E_{corr} value. Figure 4 shows the E_{corr} data for 304B4, 304B5, and 304B6 under aeration and after switching to a N_2 purge. The E_{corr} increases with time under aeration into the passive region. The negative excursions are localized corrosion initiations. The 304B6 specimen showed much more activity than the lower boron-containing alloys. The 304B4 specimen showed more negative direction spikes than the 304B5 specimen. After switching the gas flow to N_2 the potential dropped to below -0.3 V versus SCE.

The LPR calculated corrosion rates under N_2 purge were determined prior to the PS test using three LPR curves. The average corrosion rates were 221 ± 70 nm/yr for 304B4, 427 ± 132 nm/yr for 304B5, and 464 ± 100 nm/yr for 304B6.

The electrochemical potential chosen for the PS tests was based on E_{corr} measurements performed for 24 hours while the solution was saturating with air. The tests shown here were performed at 0.1 V versus SCE. The PS curves for the three Frade A alloys are shown in Figure 5. The alloys with lower boron content (304B4, 304B5) show passivation during the test while the 304B6 shows significantly higher current, particularly at the end of the test where crevice corrosion was observed. This specimen

was coated with an iron-oxide film after the test. While small pits were observed under the MCA crevice formers of the 304B6 specimen, the most significant corrosion was observed at the PTFE compression fitting used to isolate the specimen electrical contact. The corrosion rates calculated from i_{corr} were 27.0 nm/yr for 304B4 and 5.63 μm/yr for 304B6. The 304B5 specimen showed a very small negative current (1.03 x10^{-11} A) and thus no corrosion rate could be calculated. One PS experiment was performed for 304B5 with PTFE MCA washers at 0.1 V versus SCE. Figure 6 shows significant current increase initiated during the test that was consistent with crevice corrosion under the MCA in post-test inspection. The corrosion rate based on i_{corr} was 22.7 μm/yr.

Figure 7 shows SEM images of isolated areas of corrosion underneath creviced areas of a 304B4 specimen after PS testing. This type of damage was typical of the Grade A materials using ceramic washers except for the 304B6 material where more significant damage was observed.

Long term E_{corr} tests

Figure 8 shows a plot of E_{corr} versus time for specimens 304B5 and 304B6 in solution B3 with ceramic MCA washers. The potential of both specimens rose in the initial hours to over 0 V, with 304B6 attaining the more positive value. The 304B6 specimen also had numerous negative spikes due to localized corrosion. After 2 weeks, some of the negative spikes are up to 0.3 V in magnitude and last for many hours. The 304B5 specimen showed few negative excursions comparatively. After 1 week, two LPR scans were performed on the 304B6 specimen while under aeration. The corrosion rate was 80 ± 3 nm/yr, indicating very low general corrosion rate in the passive region compared to those measured under N_2 purge in the PS tests, where the E_{corr} values were near -0.3 V versus SCE. The lower corrosion rate is due to the specimen residing in the passive region when aerated. After the tests, the specimen was examined with LOM, as shown in Figure 9. The most significant damage was observed at the PTFE compression gasket (gasket for the specimen contact), where significant pitting around the circumference of the gasket was observed. Other less extensive pitting damage was observed under the MCA crevice formers. No significant damage to the 304B5 specimen with a ceramic MCA was observed.

An additional E_{corr} test using a 304B5 specimen was performed with a PTFE MCA and showed more negative excursions and a final potential that exceeded 0.2 V. This specimen did show limited crevice corrosion damage under the crevice washer.

Post-test analysis

Figure 10 shows OPM images acquired on specimens after corrosion testing. Figures 10A shows damage from a PS test for 304B4 under the PTFE MCA. Figure 10A shows the edge of a crevice corrosion pit where islands of material, on the same level as the polished surface, remain. These islands are likely secondary-phase particles (borides) that had not been released from the surface as the stainless steel austenite matrix was etched around them. Figure 10B shows the extensive crevice corrosion damage to 304B6 at the PTFE compression gasket during exposure to solution B3 at 60ºC at E_{corr}. The vertical relief is approximately 40 μm at the edge to the crevice site.

Prior work has identified the composition of the borides found in Grade A material to be a Cr_2B type with a composition in weight percent of Cr-46, Fe-40, Mn-3.5, Ni-1.0 and B-9.5 and a compound formula of $(Cr.53.Fe.42.Mn.04.Ni.01)_2B$.[6] Reported results for Grade B ingot-metallurgy material identify the borides as a M_2B type where M is a metal[12] with a chromium level of approximately 50% and iron at about 40%. Prior analysis identified the borides in an A978 material as $(Fe,Cr,Ni,Mn,Mo)_2(B,C)$.[13] The higher chromium level in the borides will deplete the base metal austenite next to the boride of this element.[5]

There was not enough corrosion product detected on the surfaces of the Grade A borated stainless steel specimens to perform suitable analysis. A representative SEM image of the damage in the crevice corrosion region under a PTFE gasket used for attachment of the electrical contacts is shown in Figures 11. The particles are the chromium-rich borides, and the corrosion mechanism appears to be localized corrosion around the borides, which allows them to fall free from the surface. The test solutions were filtered to gather a sample for XRD analysis, but the measurement results were inconclusive due to a very small sample size. Accelerated testing was used to produce adequate corrosion product in a reasonable time for analysis.

Corrosion product analysis

To increase the amount of corrosion product for XRD analysis, an accelerated corrosion test was performed using a 304B6 crevice-corrosion specimen polarized above the expected E_{corr} value (0.4 V versus SCE) at 90ºC for 24 hours in solution B3. The 304B6 alloy was chosen as it shows a reduced resistance to localized corrosion compared to alloys 304B4 and 304B5. This resulted in an excessive amount of crevice corrosion product that clouded the solution significantly (see Figure 27) and resulted in catastrophic attack to all surfaces of the specimen. The precipitate and corrosion product on the specimen was black and mostly lacked additional color. A total charge of 5616 C (355.4 C/cm^2) was passed during the test, with a maximum current of 5.29 A/cm^2 and a minimum of 2.25 A/cm^2. Thus, localized corrosion was initiated rapidly and remained active throughout the test. The descaled specimen lost 1.83141 g during the test. The precipitate was collected during descaling, with sonication in 10% HNO_3. After descaling, the specimen continued to produce small grey particles (assumed to be boride particles) upon shaking. This was presumably due to the preferential etching of the austenite matrix around the particles leaving them in corrosion cavities in the specimen. The particles removed during descaling were analyzed by XRD and matched with $FeCr_2B$. A similar match was made with a significant amount of settled precipitate collected at the bottom of the corrosion flask, which also indicated significant amounts of amorphous material.

CONCLUSIONS

Corrosion testing of four neutron-absorbing alloys, Type 304B4 Grade A, Type 304B5 Grade A, Type 304B6 Grade A, and A978 ingot metallurgy (Grade B), was performed using various electrochemical testing methods. The testing conditions were based on those expected inside a MGR waste package, should the outer barrier breach and the internals be exposed to moisture.

CPP tests were performed to determine the localized characteristics of the materials. All specimens showed breakdown behavior prior to the anodic limit (0.8 V). The ingot metallurgy specimen (A978) showed the lowest performance with the largest anodic current and lowest E_{rp} value. The powder product materials (Grade A) generally behaved as expected, with performance decreasing with the amount of B present. All specimens showed significant crevice corrosion under the MCA washers.

PS tests showed that the Grade A materials were mostly stable when held near the aerated E_{corr} values. E_{corr} testing for 24 hours showed negative spikes due to localized corrosion primarily for 304B6 with less for 304B4 and 304B5. 304B4 and 304B5 specimens showed passivation behavior with very low current and associated corrosion rates observed at the end of the tests. The exception was 304B6 which experienced an increase in current due to crevice corrosion at the end of the test. In a separate test, a 304B5 specimen also showed a significant increase in crevice corrosion under a PTFE MCA washer. Thus the crevice former was an important variable to consider.

Long-term E_{corr} testing was performed on two specimens for several weeks to determine the long-term E_{corr} behavior. Both specimens trended positive initially and equilibrated after approximately 200 hours. The 304B6 specimen showed significant corrosion signatures (negative spiking) while a 304B5 specimen showed much more stable behavior. This observation was consistent with the 24 hour aerated E_{corr} data from PS tests and the higher E_{bd} observed in PD tests.

Analysis of the surfaces following corrosion showed the tendency for corrosion to occur around the secondary phase particles. This was best observed near the interface of crevice corrosion pits where islands of boride particles remained. The observation of etching of the austenite matrix surrounding the boride particles is in agreement with previous studies of borated stainless steels.[7,9]

Corrosion product analysis was performed on one 304B6 specimen treated to an aggressive condition in a representative chemistry. Extensive breakdown was observed with a cloudy solution and significant corrosion buildup on the surface. After specimen descaling and filtering the remaining particles were found to be $(FeCr)_2B$. Corrosion product that settled to the bottom of the flask also contained boride particles along with significant amorphous material.

The secondary-phase $(FeCr)_2B$ of the borated stainless steel appears to be stable, thus, do not contribute to the corrosion directly. The secondary phase (boride) particles are known to reduce the overall localized corrosion properties due to chromium depletion from the austenite phase adjacent to the boride [5-6,12] The fate of the secondary phase particles is also of great interest as this contains the neutron absorbing element. These tests have shown that the boride particles are either contained in the corrosion film or fall to the bottom of the flask. Since these particles are small one would expect some mobility. There is also the question of the solubility of the boron. Previous corrosion testing briefly mentions slight attack of these boride particles.[7,9] Due to the small size and irregular shape of these particles is it difficult to make any conclusions on what happens to these particles from this data. It is known that some particles stay in the specimen after corrosion while other fall from the suspended specimen.

This work has shown that more work is needed to ascertain the fate of the boride particles and also determine possible transport mechanisms if credit is taken for them remaining as viable inside the waste package. This work has also shown that the Grade A borated stainless steels are very close to the edge of stability to localized corrosion under these conditions, leaving little margin for unanticipated conditions.

ACKNOWLEDGEMENTS

This work was performed by the Idaho National Laboratory for the U.S. Department of Energy, Office of Civilian Radioactive Waste Management, under DOE Idaho Operations Office Contract DE-AC07-051D14517.

TABLE 1

ALLOY COMPOSITION (WT%) FOR BORATED STAINLESS STEEL SPECIMENS

	304B4 Grade A	304B5 Grade A	304B6 Grade A	A978 ingot
Heat #	182194	182195	182196	E084295
Name	304B4	304B5	304B6	A978
Cr	19.46	19.36	19.04	18.18
Ni	13.39	13.39	12.78	12.07
Mo	-	-	-	2.11
B	1.17	1.32	1.69	1.00
Gd	-	-	-	-
C	0.05	0.05	0.05	0.056
Mn	1.91	1.84	1.69	1.70
Cu	-	-	-	0.35
Fe	Bal	Bal	Bal	Bal

TABLE 2

SOLUTION COMPOSITIONS USED FOR TESTING

Test Solution	$[Cl^-]$ (m)	$[F^-]$ (m)	$[NO_3^-]$ (m)	pH	NO_3/Cl	$NO_3/(Cl+F)$
B1	0.004	0	0.005	7	1.25	1.25
B3	0.004	0.001	0.0025	5.5	0.63	0.50

TABLE 3

PARAMETERS OBTAINED FROM CPP CURVES IN SOLUTION B1

	304B4	304B5	304B6	A978
E_{corr}	-0.28	-0.3034	-0.3347	-0.291
E_{bd}	0.25	0.321	0.207	0.055
E_{rp}	0.022	0.018	-0.0943	-0.115

TABLE 4

PARAMETERS OBTAINED FROM CPP CURVES IN SOLUTION B3

	304B4	304B5	304B6
E_{corr}	-0.3031	-0.3283	-0.3728
E_{bd}	0.351	0.429	0.353
E_{rp}	0.032	-0.052	-0.137

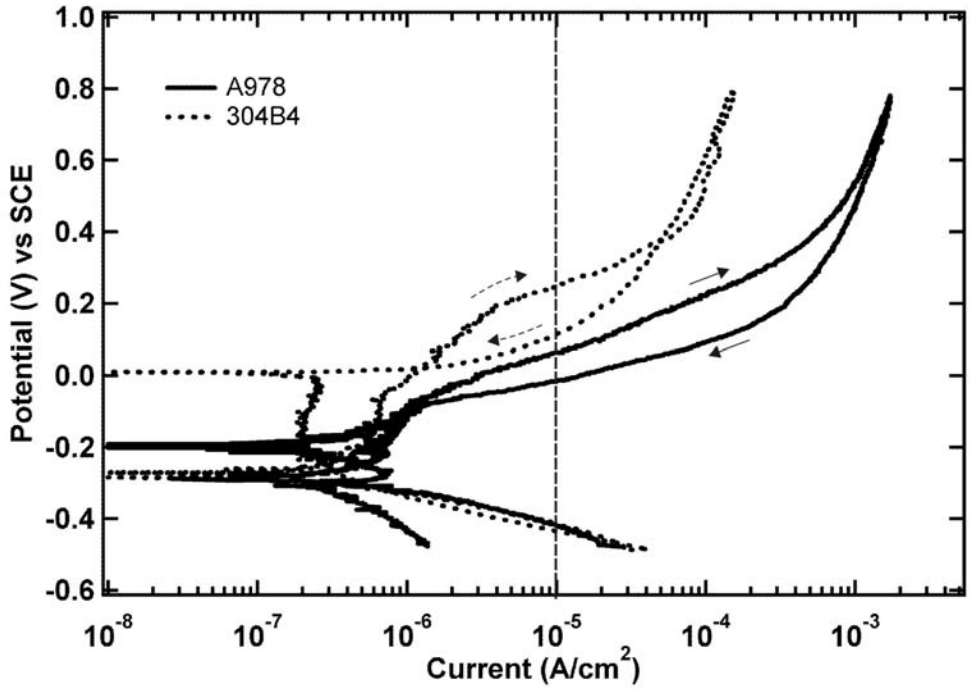

FIGURE 1 - CPP curves for A978 and 304B4 specimens in solution B1 at 60ºC.

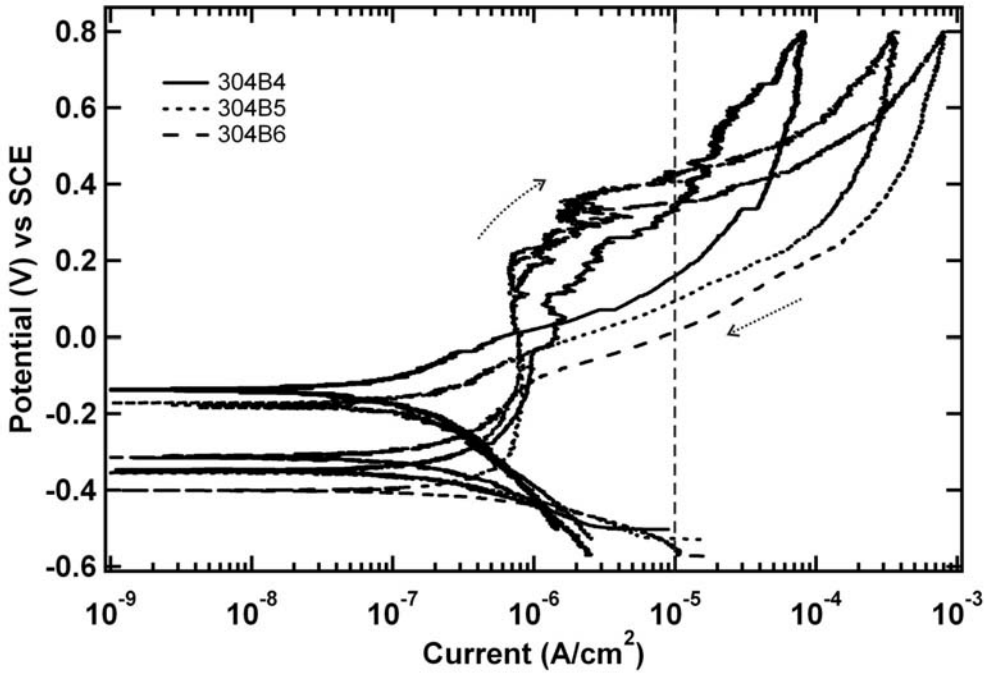

FIGURE 2 - CPP curves for Grade A alloys in solution B3 at 60ºC using PTFE multiple crevice assembly (MCA) crevice formers.

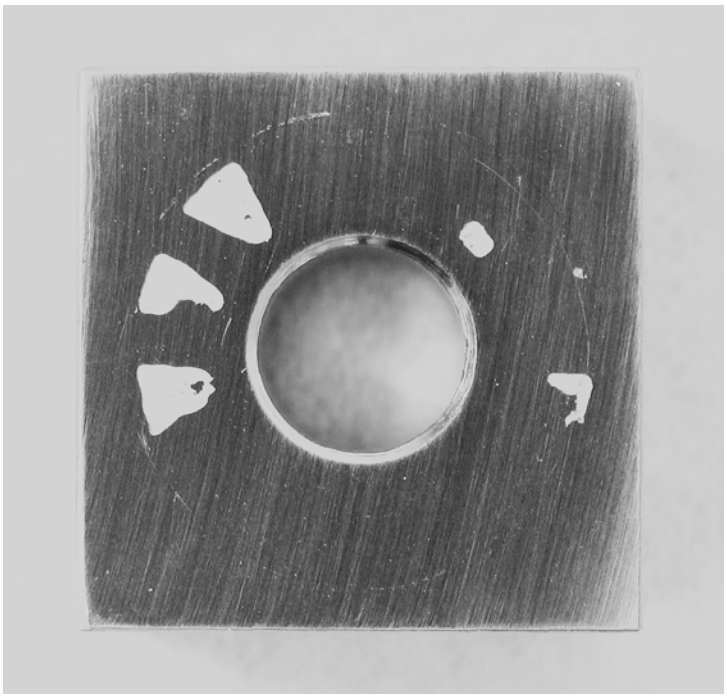

FIGURE 3 - Photograph of 304B4 specimen after a CPP scan in B1 solution (See Figure 1).

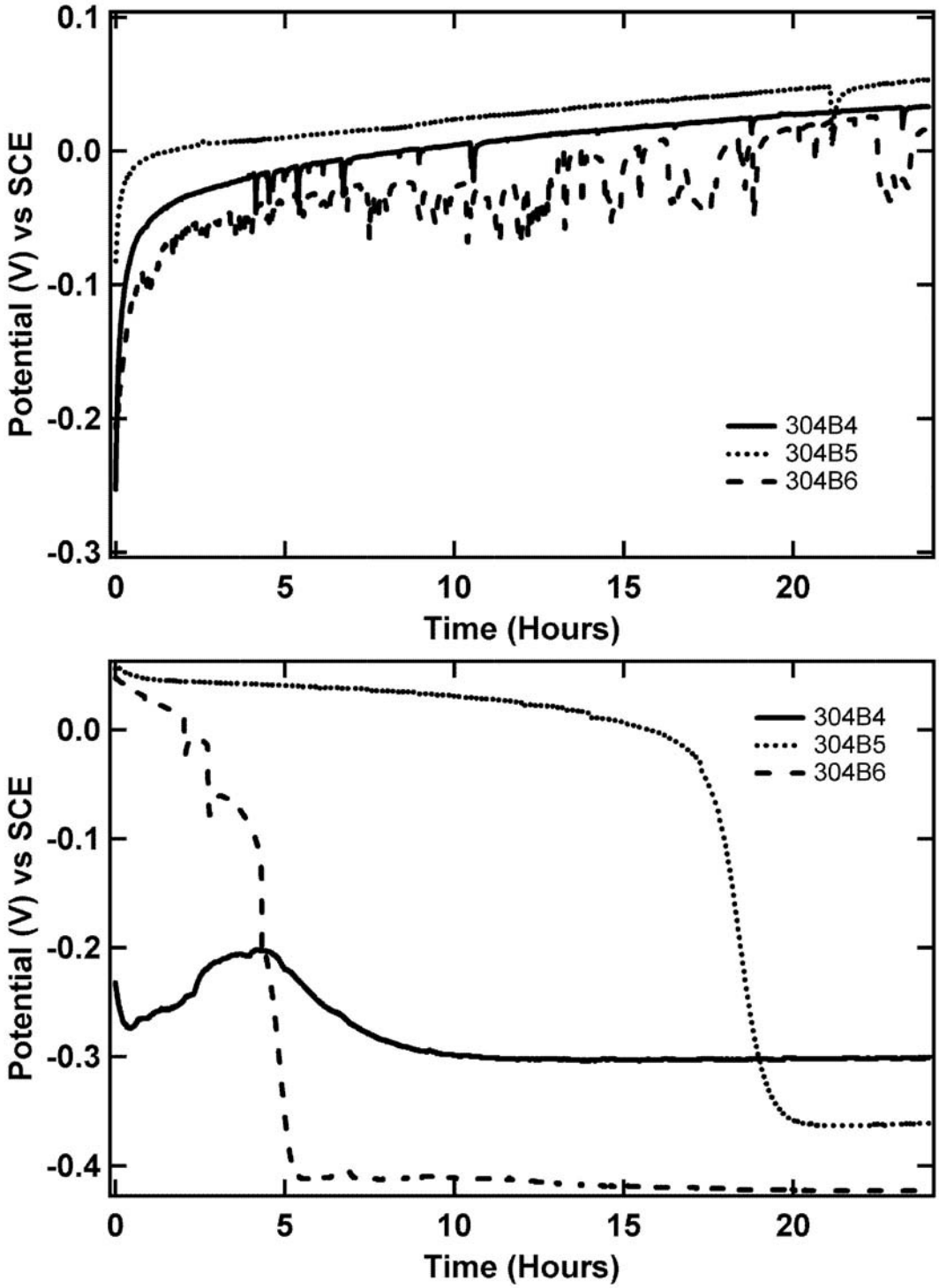

FIGURE 4 - E_{corr} for 304B4, 304B5, and 304B6 in solution B3 at 60ºC with air (top) and N_2 (bottom) purge.

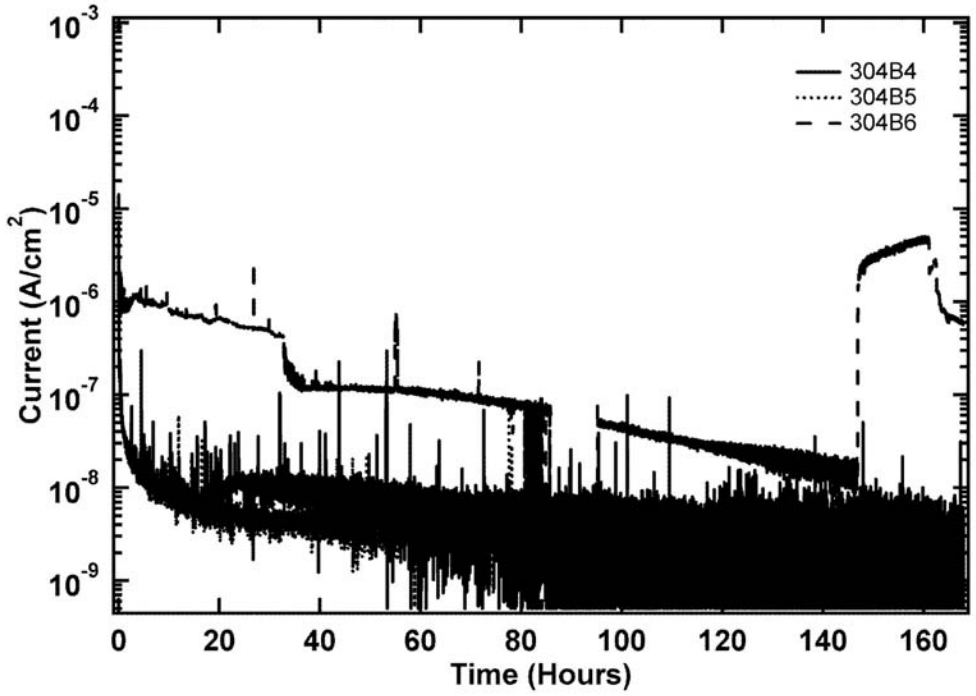

FIGURE 5 - PS curves for 304B4, 304B5, and 304B6 in solution B3 with ceramic MCA.

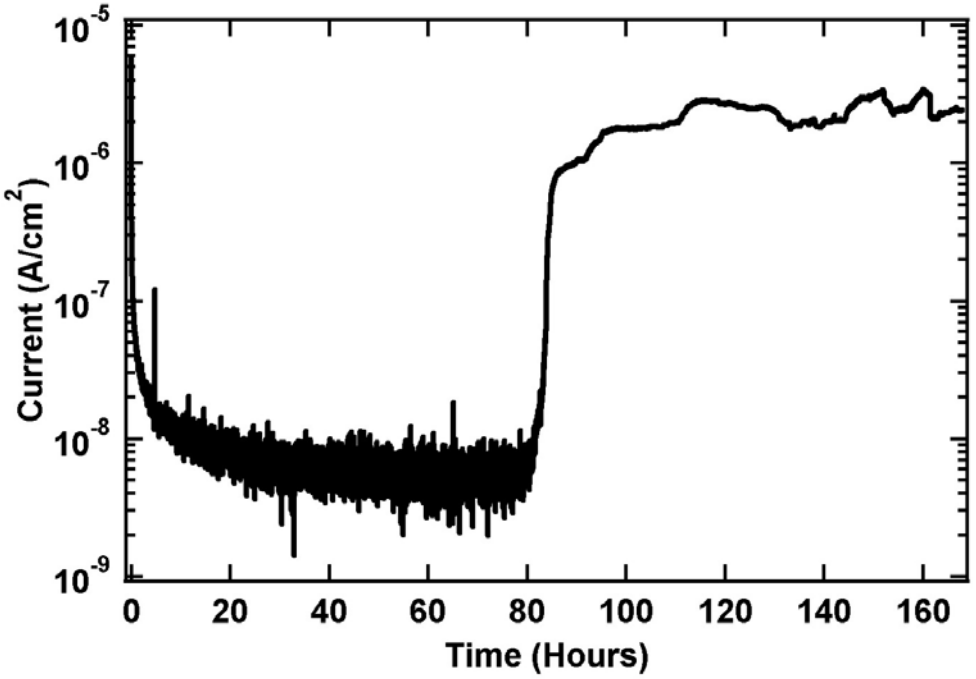

FIGURE 6 - PS curve for 304B5 in solution B3 with PTFE MCA.

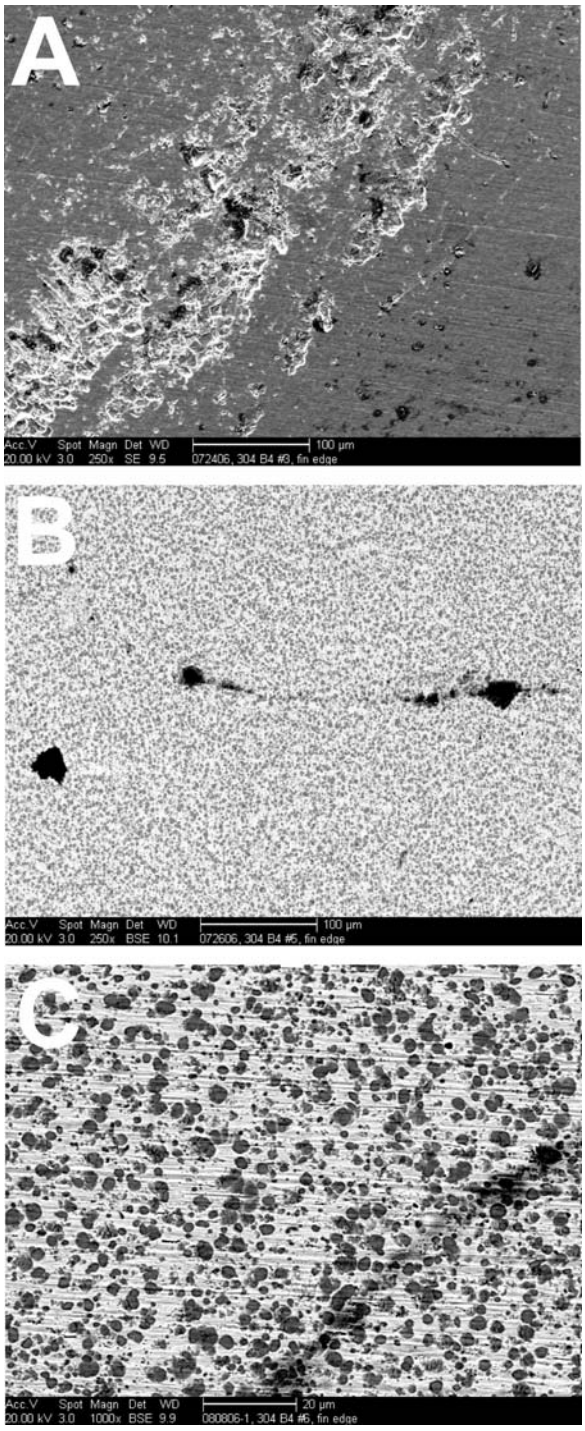

FIGURE 7 – SEM images of 304B4 specimen following PS tests. Images A was taken in SE mode and images B-C were taken in BSE mode where darker grey areas are the boride phase and black areas corrosion sites.

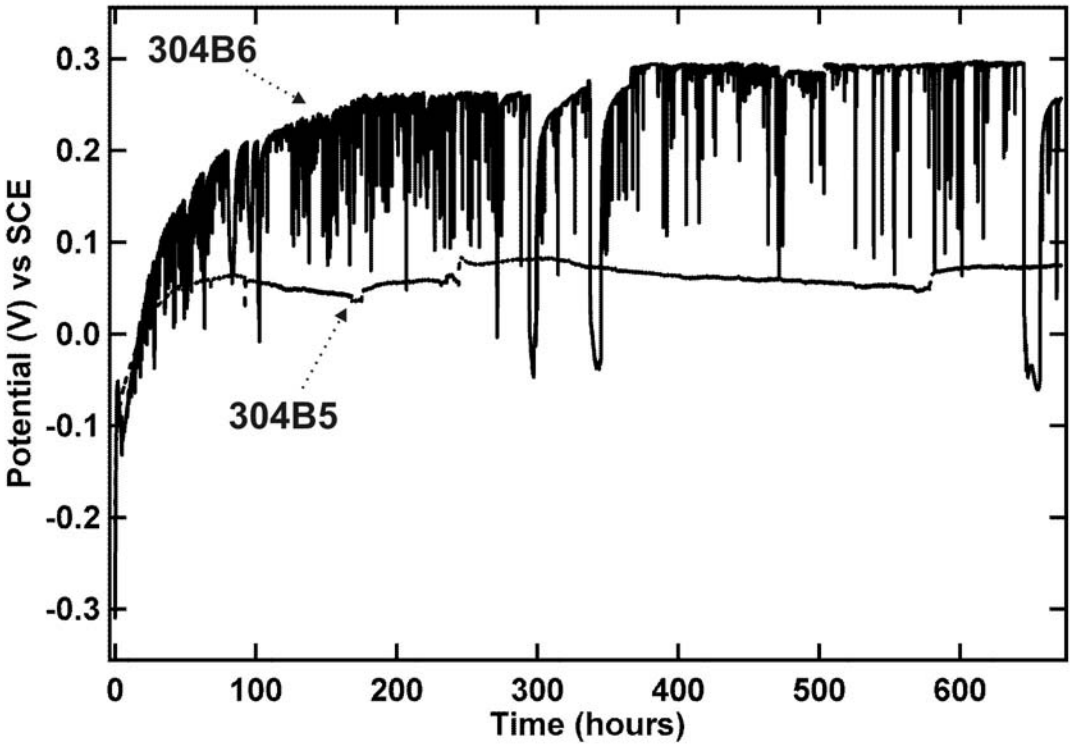

FIGURE 8 - E_{corr} versus time for 304B5 and 304B6 specimens in solution B3 at 60ºC.

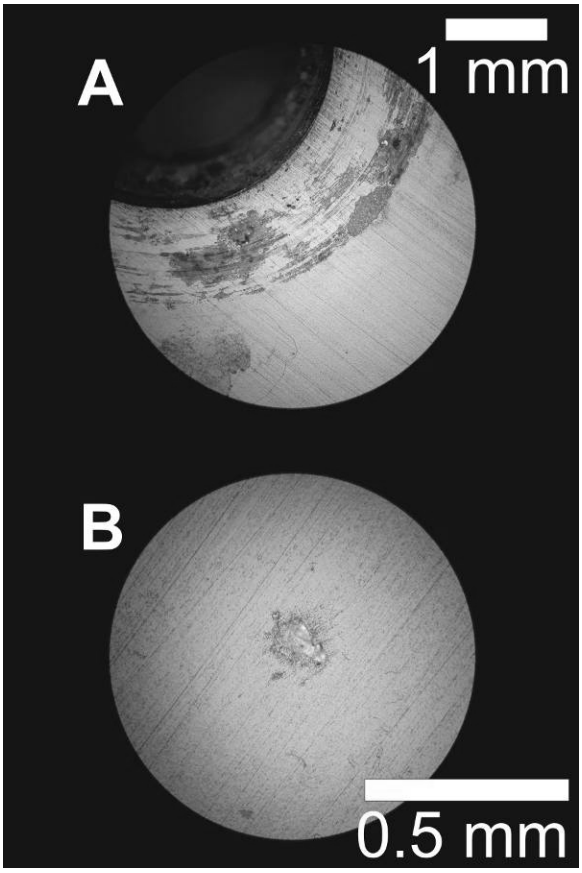

FIGURE 9 - LOM of 304B6 specimen after 4 weeks at E_{corr}. Image (A) was taken from a compression gasket (50X) and image (B) was taken from an area under the ceramic MCA crevice former (200X). Note that the dark area in the upper left corner of (A) is the tapped hole for the contact rod.

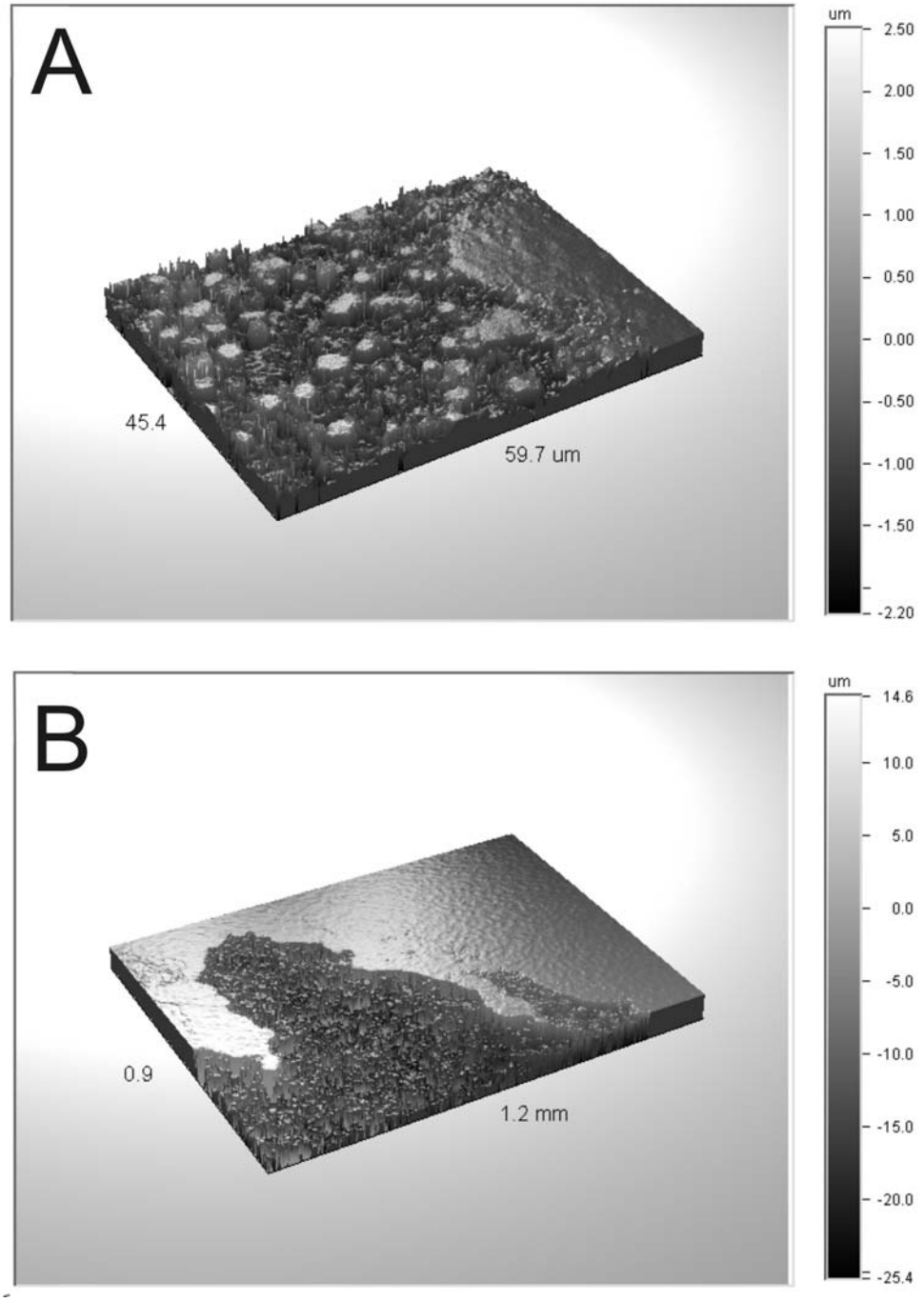

FIGURE 10 – OPM image of specimens after corrosion experiments. (A) near the edge of crevice corrosion pit on a 304B4 specimen after PS test in solution B3 and (B) 304B6 specimen showing crevice corrosion under the PTFE compression fitting (specimen electrical connection gasket) after a long-term E_{corr} test in solution B3.

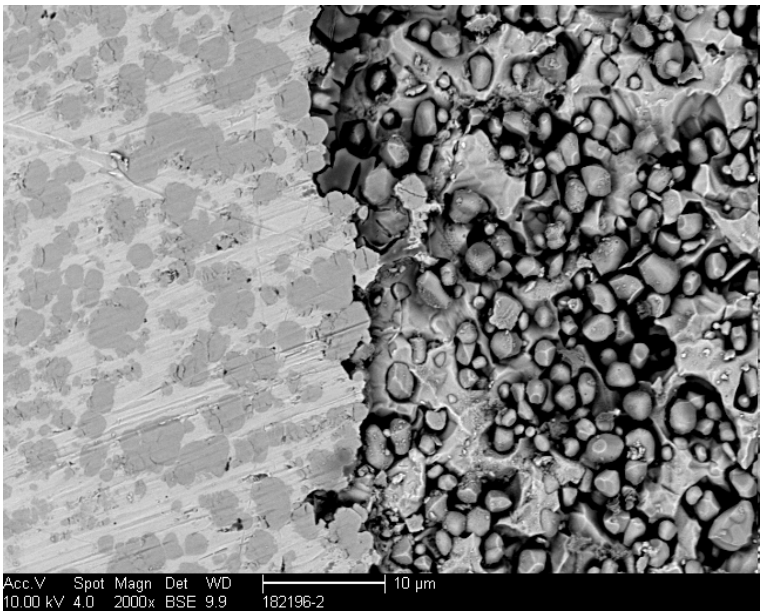

FIGURE 11 - SEM image taken in BSE made showing morphology at the edge of large crevice corrosion site in 304B6. The left side shows the undamaged surface and the right shows the creviced area with exposed borides.

REFERENCES

1 DOE 2007, "Transportation, Aging, and Disposal Canister System Performance Specification", DOE/RW-0585, Rev. 0, June 2007.

2. ASTM A887-89, "Standard Specification for Borated Stainless Steel Plate, Sheet, and Strip for Nuclear Application*,*"American Society for Testing and Materials, 2004.

3. K. Wasinger, "High Density Spent Fuel Storage in Spain-Capacity for the Entire Life," *Nuclear Plant Journal*, July-August 1993, p. 46.

4. D.G. Abbott and R.E. Nickell, "Experience with Certifying Borated Stainless Steel as a Shipping Cask Material," *1st International Topical Meeting on High-Level Radioactive Waste Management, Las Vegas, NV, April 1990*.

5. H.J. Goldschmidt, "Effect of Boron Additions to Austenitic Stainless Steels Part II, Solubility of Boron in 18% Cr, 15% Ni Austenitic Steel," *Journal of the Iron and Steel Institute*, November 1971, p. 910.

6. J.W. Martin, "Effects of Processing and Microstructure on the Mechanical Properties of Boron-Containing Austenitic Stainless Steels," *Proceedings Symposium Waste Management, University of Arizona, AZ, 1989,* p. 293.

7. D.A. Moreno, B. Molina, C. Ranninger, F. Montero, and J. Izquierdo, "Microstructural Characterization and Pitting Corrosion Behavior of UNS S30466 Borated Stainless Steel," *Corrosion* 60, 6 (2004) 573.

8. R.S. Brown, Corrosion Resistance of Borated Stainless Steels, Carpenter Technology Corp., March 1991.

9. D.V. Fix, J.C. Estill, L.L. Wong, and R.B. Rebak, "General and Localized Corrosion of Austenitic and Borated Stainless Steels in Simulated Concentrated Ground Waters," *American Society of Mechanical Engineers Pressure Vessels and Piping Division (ASME-PVP) Conference, San Diego, CA, July 2004*.
10. ASTM G5-94, "Standard Reference Test Method for Making Potentiostatic and Potentiodynamic Anodic Polarization Measurements," American Society for Testing and Materials, 2004.
11. ASTM G102-89, "Standard Practice for Calculation of Corrosion Rates and Related Information from Electrochemical Measurements," American Society for Testing and Materials, 2004.
12. E.A. Loria and H.S. Isaacs, "Type 304 stainless Steel with 0.5% Boron for Storage of Spent Nuclear Fuel", *Journal of Metals*, December 1980, p. 10.
13. A. Kugler, Neutronit A976, Sheet and Plate for Nuclear Engineering, Bohler Bleche GmbH, September 1997.